
Article:
Feline, W.J., Dhillon, V.S., Marsh, T.R. et al. (2004) ULTRACAM photometry of the eclipsing cataclysmic variables XZ Eri and DV UMa. Monthly Notices of the Royal Astronomical Society, 355 (1). pp. 1-10. ISSN: 0035-8711

https://doi.org/10.1111/j.1365-2966.2004.08302.x

Mon. Not. R. Astron. Soc. **355,** 1–10 (2004) doi:10.1111/j.1365-2966.2004.08302.x

ULTRACAM photometry of the eclipsing cataclysmic variables XZ Eri and DV UMa

W. J. Feline,[1⋆] V. S. Dhillon,[1] T. R. Marsh[2] and C. S. Brinkworth[3]

[1]*Department of Physics and Astronomy, University of Sheffield, Sheffield S3 7RH*
[2]*Department of Physics, University of Warwick, Coventry CV4 7AL*
[3]*Department of Physics and Astronomy, University of Southampton, Southampton SO17 1BJ*

Accepted 2004 August 6. Received 2004 July 22; in original form 2004 April 30

ABSTRACT

We present high-speed, three-colour photometry of the faint eclipsing cataclysmic variables XZ Eri and DV UMa. We determine the system parameters through two techniques: first, timings of the eclipse contact phases of the white dwarf and bright-spot using the derivative of the light curve; and secondly, a parametrized model of the eclipse fitted to the observed light curve by χ^2 minimization. For both objects, we prefer the latter method, as it is less affected by photon noise and rapid flickering. For XZ Eri we obtain a mass ratio $q = 0.1098 \pm 0.0017$ and an orbital inclination $i = 80\overset{\circ}{.}16 \pm 0\overset{\circ}{.}09$. For DV UMa we derive figures of $q = 0.1506 \pm 0.0009$ and $i = 84\overset{\circ}{.}24 \pm 0\overset{\circ}{.}07$. The secondary star in XZ Eri has a very low mass $M_{\rm r}/{\rm M}_{\odot} = 0.0842 \pm 0.0024$, placing it close to the upper limit on the mass of a brown dwarf.

Key words: binaries: close – binaries: eclipsing – stars: dwarf novae – stars: individual: DV UMa – stars: individual: XZ Eri – novae, cataclysmic variables.

1 INTRODUCTION

Cataclysmic variable stars (CVs) are a class of interacting binary systems undergoing mass transfer via a gas stream and accretion disc from a Roche lobe filling secondary to a white dwarf primary. A bright-spot is formed at the intersection of the disc and gas stream, giving rise to an 'orbital hump' in the light curve at phases 0.6–1.0 due to foreshortening of the bright-spot. The light curves of eclipsing CVs can be quite complex, with the accretion disc, white dwarf and bright-spot all being eclipsed in rapid succession. With sufficient time resolution, however, this eclipse structure allows the system parameters to be determined to a high degree of accuracy. Warner (1995) gives a comprehensive review of CVs.

The class of CVs known as the dwarf novae intermittently undergo outbursts – increases in brightness of between two and five magnitudes. Both XZ Eri and DV UMa are members of the SU UMa subclass of dwarf novae, which also exhibit superoutbursts (about 0.7 mag brighter than normal outbursts) at semiregular intervals.

XZ Eri was first noted to be variable by Shapley & Hughes (1934). Until recently (Howell et al. 1991; Szkody & Howell 1992), however, XZ Eri had been rather poorly studied. The presence of eclipses in the light curve of XZ Eri was discovered by Woudt & Warner (2001). More recently, Uemura et al. (2004) observed superhumps in the outburst light curve of XZ Eri, confirming its classification as an SU UMa star.

Previous observations of DV UMa are summarized by Nogami et al. (2001), who also present light curves obtained during the 1995 outburst and the 1997 superoutburst. Patterson et al. (2000) present superoutburst and quiescent photometry, from which they derive the system parameters. Mukai et al. (1990) estimated the spectral type of the secondary star to be ∼M4.5 from spectroscopic observations.

In this paper we present simultaneous three-colour, high-speed photometry of XZ Eri and DV UMa. We derive the system parameters via two separate methods – timings of the eclipse contact phases and fitting a parametrized model of the eclipse – and discuss the relative merits of each.

2 OBSERVATIONS

XZ Eri and DV UMa were observed simultaneously in three colour bands using ULTRACAM (Dhillon & Marsh 2001; Dhillon et al., in preparation) on the 4.2-m William Herschel Telescope (WHT) at the Isaac Newton Group of Telescopes, La Palma. The observations are summarized in Table 1. Data reduction was carried out as described in Feline et al. (2004) using the ULTRACAM pipeline data reduction software. The resulting light curves of XZ Eri and DV UMa are shown in Figs 1 and 2, respectively. The observations of XZ Eri began at high airmass (1.8) – this is evident in the improved quality of the second cycle. Note also that the XZ Eri data of 2003 November 13 have significantly worse time resolution than those of DV UMa, despite both objects being of similar magnitude. This is due to the higher brightness of the sky on 2003 November 13.

3 LIGHT-CURVE MORPHOLOGY

The light curve of XZ Eri shown in Fig. 1 is a classic example of an eclipsing dwarf nova. Between phase −0.4 and the start of eclipse,

⋆E-mail: w.feline@shef.ac.uk

Table 1. Journal of observations. Observing conditions were clear except for 2003 May 20, when thin cirrus was present. The dead-time between exposures was 0.025 s for all the DV UMa observations, and 0.024 s for the XZ Eri observations.

Date	Cycle	Target	Filters	Exposure time (s)	Data points	Eclipses	Seeing (arcsec)	Airmass
2003 May 20	69023	DV UMa	u', g', i'	5.921	339	1	1.3–2.0	1.5–1.8
2003 May 22	69046	DV UMa	u', g', i'	4.921	345	1	1.2	1.4–1.5
2003 May 23	69058	DV UMa	u', g', i'	4.921	60	0	1.0	1.6–1.9
2003 May 23	69058	DV UMa	u', g', i'	3.921	540	1		
2003 Nov 13	4733/4734	XZ Eri	u', g', r'	6.997	1225	2	1.0–2.0	1.4–1.8

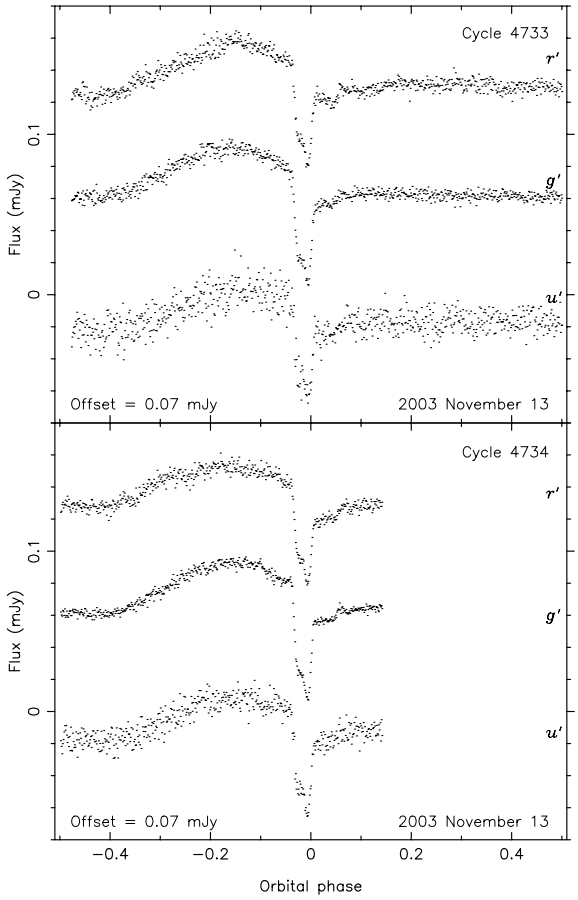

Figure 1. The light curve of XZ Eri. The data are contiguous. The r' data are offset vertically upwards and the u' data are offset vertically downwards.

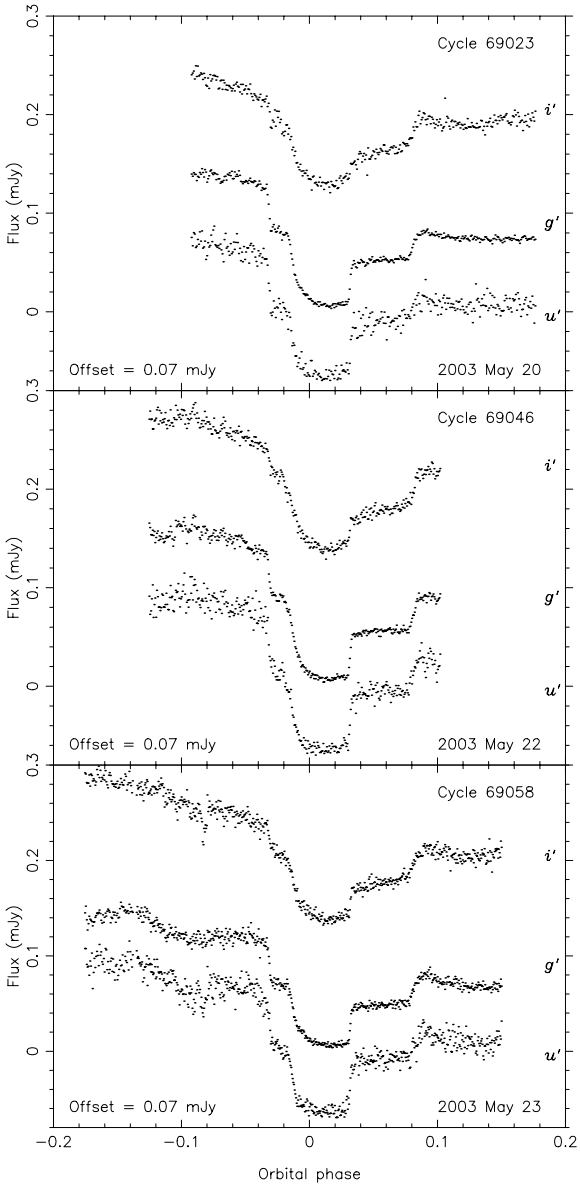

Figure 2. The light curve of DV UMa. The i' data are offset vertically upwards and the u' data are offset vertically downwards.

the orbital hump is clearly visible, with a brightening in g' flux of 0.025 mJy (0.5 mag). The light curve clearly shows separate eclipses of the white dwarf and bright-spot in all three colour bands.

During our observations, XZ Eri had $g' \sim 19.5$, falling to $g' \sim 21.5$ in mid-eclipse. Comparing this to the previous (quiescent) observations of Woudt & Warner (2001), who observed the system at $V \sim 19.2$, confirms that XZ Eri was in quiescence at the time of our observations.

The light curve of DV UMa is presented in Fig. 2. Although the phase coverage is less complete than for XZ Eri, the eclipse morphology is again typical of eclipsing short-period dwarf novae. The white dwarf and bright-spot ingress and egress are both clear and distinct. The orbital hump in DV UMa is much less pronounced than in XZ Eri.

Howell et al. (1988) quoted $V \sim 19.2$ in quiescence for DV UMa. This compares to $g' \sim 19$ at the time of our observations, which fell to $g' \sim 22$ during eclipse. DV UMa was therefore in quiescence over the course of our observations.

4 ORBITAL EPHEMERIDES

The times of white dwarf mid-ingress $T_{\rm wi}$ and mid-egress $T_{\rm we}$ were determined by locating the times when the minimum and maximum values, respectively, of the light-curve derivative occurred (Wood, Irwin & Pringle 1985). The times of mid-eclipse $T_{\rm mid}$ given in Table 2 were determined by assuming the white dwarf eclipse to be symmetric around phase zero and taking $T_{\rm mid} = (T_{\rm we} + T_{\rm wi})/2$.

To determine the orbital ephemeris of XZ Eri we used the one mid-eclipse time of Woudt & Warner (2001), the 25 eclipse timings of Uemura et al. (2004) and the six times of mid-eclipse given in Table 2. We used errors of 5×10^{-4} d for the Woudt & Warner (2001) data, 1×10^{-4} d for the Uemura et al. (2004) timings and 4×10^{-5} d for the ULTRACAM data. A linear least-squares fit to these times gives:

$$\begin{array}{l}\mathrm{HJD} = 245\,2668.040\,99 + 0.061\,159\,491\,E.\\ \qquad\qquad\qquad\quad 2\pm \qquad\qquad 5\end{array}$$

The orbital ephemeris of DV UMa was determined in a similar way using the 18 mid-eclipse timings of Nogami et al. (2001), the 12 timings of Howell et al. (1988), the 12 timings of Patterson et al. (2000) and the nine times of mid-eclipse given in Table 2, with errors of 5×10^{-4} d assigned to the data of Nogami et al. (2001) and Howell et al. (1988), 1×10^{-4} d to the data of Patterson et al. (2000) and 4×10^{-5} d to the ULTRACAM data. A linear least-squares fit to these times gives:

$$\begin{array}{l}\mathrm{HJD} = 244\,6854.661\,57 + 0.085\,852\,6521\,E.\\ \qquad\qquad\qquad\quad 9\pm \qquad\qquad 14\end{array}$$

These ephemerides were used to phase all of our data.

Table 2. Mid-eclipse timings (HJD + 245 2000).

XZ Eri cycle	u'	g'	r'
4733	957.508 910	957.508 789	957.508 870
4734	957.570 081	957.570 000	957.570 000
DV UMa cycle	u'	g'	i'
69023	780.469 225	780.469 225	780.469 225
69046	782.443 801	782.443 829	782.443 801
69058	783.474 062	783.474 040	783.474 040

5 LIGHT-CURVE DECOMPOSITION

5.1 The derivative method

This method of determining the system parameters of an eclipsing dwarf nova was originally developed by Wood et al. (1986). It relies upon the fact that there is a unique relationship between the mass ratio $q = M_{\rm r}/M_{\rm w}$ and orbital inclination i for a given eclipse phase width $\Delta\phi$ (Bailey 1979).

The eclipse contact phases given in Tables 3 and 4 were determined using the derivative of the light curve, as described by Feline et al. (2004, and references therein). The mid-points of ingress and egress are denoted by $\phi_{\rm i}$ and $\phi_{\rm e}$, respectively. The eclipse contact phases corresponding to the start and end of the ingress are denoted by ϕ_1 and ϕ_2, and the start and end of the egress by ϕ_3 and ϕ_4. In the discussion that follows, we use the suffixes 'w' and 'b' to denote white dwarf and bright-spot contact phases, respectively (e.g. $\phi_{\rm wi}$ means the mid-point of the white dwarf ingress). The eclipse phase full width at half-depth is $\Delta\phi = \phi_{\rm we} - \phi_{\rm wi}$. In the following analysis we have combined the timings of all three colour bands for each target in order to increase the accuracy of our results.

The mass ratio – and hence the inclination – may be determined by comparing the bright-spot light centres corresponding to the measured eclipse contact phases $\phi_{\rm bi}$ and $\phi_{\rm be}$ with the theoretical stream trajectories for different mass ratios. As illustrated in Fig. 3, the assumption that the gas stream (originating from the inner Lagrangian point L_1) passes directly through the light centre of the bright-spot at the edge of the disc allows the determination of the mass ratio, orbital inclination and relative outer disc radius $R_{\rm d}/a$ (where a is the orbital separation).

For the mean eclipse phase width of $\Delta\phi = 0.035\,889$, the eclipse timings of XZ Eri (Tables 3 and 4) yield the mass ratio, inclination and relative disc radius given later in Table 7. The results for

Table 3. White dwarf contact phases and out-of-eclipse white dwarf fluxes. We estimate that the errors on the fluxes are ±0.001 mJy.

Cycle	Band	$\phi_{\rm w1}$	$\phi_{\rm w2}$	$\phi_{\rm w3}$	$\phi_{\rm w4}$	$\phi_{\rm wi}$	$\phi_{\rm we}$	Flux (mJy)
XZ Eri								
4733	u'	−0.020 996	−0.015 625	0.016 113	0.022 461	−0.018 555	0.018 555	0.0434
	g'	−0.022 461	−0.011 719	0.012 207	0.020 020	−0.018 555	0.017 578	0.0466
	r'	−0.022 461	−0.013 184	0.013 184	0.020 020	−0.019 531	0.016 113	0.0441
4734	u'	−0.018 066	−0.014 160	0.010 742	0.020 020	−0.017 090	0.017 578	0.0341
	g'	−0.022 461	−0.013 184	0.013 672	0.021 484	−0.019 531	0.017 578	0.0531
	r'	−0.022 461	−0.013 184	0.015 137	0.020 020	−0.017 090	0.017 578	0.0375
DV UMa								
69023	u'	−0.033 850	−0.030 644	0.030 276	0.033 482	−0.031 445	0.032 680	0.0465
	g'	−0.033 850	−0.030 644	0.030 276	0.033 482	−0.031 445	0.032 680	0.0373
	i'	−0.033 048	−0.029 842	0.030 276	0.033 482	−0.030 644	0.031 879	0.0245
69046	u'	−0.032 798	−0.030 132	0.031 210	0.033 210	−0.031 465	0.031 877	0.0451
	g'	−0.033 467	−0.030 132	0.031 210	0.033 879	−0.032 132	0.032 543	0.0435
	i'	−0.032 798	−0.030 132	0.030 544	0.033 210	−0.030 799	0.031 877	0.0239
69058	u'	−0.032 691	−0.030 564	0.030 612	0.032 206	−0.030 564	0.032 206	0.0356
	g'	−0.033 224	−0.030 564	0.030 612	0.032 739	−0.031 097	0.032 206	0.0318
	i'	−0.033 755	−0.030 564	0.031 142	0.033 270	−0.032 161	0.032 739	0.0312

Table 4. Bright-spot contact phases.

Cycle	Band	ϕ_{b1}	ϕ_{b2}	ϕ_{b3}	ϕ_{b4}	ϕ_{bi}	ϕ_{be}
XZ Eri							
4733	u'	−0.000 977	0.006 836	0.064 941	0.067 871	0.002 930	0.066 406
	g'	0.000 000	0.006 836	0.069 336	0.074 219	0.003 906	0.073 242
	r'	−0.000 977	0.006 836	0.069 336	0.073 242	0.001 465	0.070 313
4734	u'	−0.000 977	0.006 836	0.063 965	0.081 055	0.002 930	0.070 801
	g'	−0.000 977	0.006 836	0.065 430	0.070 801	0.001 465	0.067 871
	r'	0.000 488	0.005 859	0.065 430	0.069 336	0.002 930	0.067 871
DV UMa							
69023	u'	−0.018 620	−0.009 803	0.079 171	0.083 179	−0.013 811	0.082 378
	g'	−0.016 215	−0.011 406	0.079 171	0.083 179	−0.013 811	0.080 775
	i'	−0.017 017	−0.009 001	0.078 370	0.085 584	−0.013 009	0.079 973
69046	u'	−0.016 797	−0.012 129	0.079 884	0.085 885	−0.014 131	0.080 553
	g'	−0.018 130	−0.010 129	0.079 884	0.084 552	−0.014 131	0.081 886
	i'	−0.022 131	−0.006 127	0.081 220	0.083 219	−0.014 797	0.081 886
69058	u'	−0.015 671	−0.009 819	0.079 019	0.080 613	−0.014 074	0.079 550
	g'	−0.015 671	−0.010 883	0.079 019	0.081 680	−0.013 541	0.079 550
	i'	−0.014 604	−0.010 883	0.077 955	0.083 274	−0.013 010	0.078 486

DV UMa for the mean eclipse phase width of $\Delta\phi = 0.063\,604$ are also given in Table 7. The errors on these parameters are determined by the rms variations in the measured contact phases. We use the bright-spot eclipse timings to determine upper limits on the angular size and the radial and vertical extents of the bright-spots, defining $\Delta\theta$, ΔR_d, ΔZ and ΔZ_2 as in Feline et al. (2004). The mean position and extent of the bright-spots thus derived are given in Table 5.

Using the mass ratio and orbital inclination given in Table 7 and the eclipse constraints on the radius of the white dwarf (Table 3), we find that the white dwarf in XZ Eri has a radius of $R_w/a = 0.012 \pm 0.002$. For DV UMa we obtain $R_w/a = 0.0075 \pm 0.0020$. We will continue under the assumption that the eclipsed central object is a bare white dwarf. This assumption and its consequences are discussed in more detail in Feline et al. (2004).

The fluxes given in Table 3 were fitted to the hydrogen-rich, $\log g = 8$ white dwarf model atmospheres of Bergeron, Wesemael & Beauchamp (1995). The colour indices quoted therein were converted to the SDSS system using the observed transformations of Smith et al. (2002). The white dwarf temperatures T_w thus calculated are given in Table 7.

To determine the remaining system parameters of XZ Eri and DV UMa, we have used the Nauenberg mass–radius relation for a cold, non-rotating white dwarf (Nauenberg 1972; Cook & Warner 1984), which gives an analytical approximation to the Hamada–Salpeter mass–radius relation (Hamada & Salpeter 1961). This relation, together with Kepler's third law and the relative white dwarf radius, allows the analytical determination of the absolute system parameters, given in Table 7. The secondary radius R_r has been calculated by approximating it to the volume radius of the Roche lobe (Eggleton 1983), which is accurate to better than 1 per cent. Because the Nauenberg mass–radius relation assumes a cold white dwarf, we have attempted to correct this to a temperature of $T_w \sim 15\,000$ K for XZ Eri and to $T_w \sim 20\,000$ K for DV UMa, the approximate temperatures given by the model atmosphere fit. The radius of the white dwarf at 10 000 K is about 5 per cent larger than for a cold (0 K) white dwarf (Koester & Schönberner 1986). To correct from 10 000 K to the appropriate temperature, the white dwarf cooling curves of Wood (1995) for $M_w/M_\odot = 1.0$, the approximate masses given by the Nauenberg relation, were used. This gave total radial corrections of 6.0 and 7.0 per cent for XZ Eri and DV UMa, respectively.

5.2 A parametrized model of the eclipse

Another way of determining the system parameters is to use a physical model of the binary system to calculate eclipse light curves for each of the various components. We used the technique developed by Horne et al. (1994) and described in detail therein. This model assumes that the eclipse is caused by the secondary star, which completely fills its Roche lobe. A few changes were necessary in order to make the model of Horne et al. (1994) suitable for our data. The most important of these was the fitting of the secondary flux, prompted by the detection of a significant amount of flux from the secondary in the i' band of DV UMa. The secondary flux is very small in all the other bands. Fitting of ellipsoidal variations made no significant improvement to the overall fit, so we have assumed the flux from the secondary star to be constant. For both XZ Eri and DV UMa we fitted this model to all the cycles, which were phase-folded and binned by two data points. Examination of the light curves shown in Figs 1 and 2 shows that cycle-to-cycle variations for both targets were minimal.

The 10 parameters that control the shape of the light curve are as follows.

(i) The mass ratio, q.
(ii) The eclipse phase full width at half-depth, $\Delta\phi$.
(iii) The outer disc radius, R_d/a.
(iv) The white dwarf limb darkening coefficient, U_w.
(v) The white dwarf radius, R_w/a.
(vi) The bright-spot scale, S/a. The bright-spot is modelled as a linear strip passing through the intersection of the gas stream and disc. The intensity distribution along this strip is given by $(X/S)^2\,e^{-X/S}$, where X is the distance along the strip.
(vii) The bright-spot tilt angle, θ_B, measured relative to the line joining the white dwarf and the secondary star. This allows adjustment of the phase of the orbital hump.
(viii) The fraction of bright-spot light that is isotropic, f_{iso}.

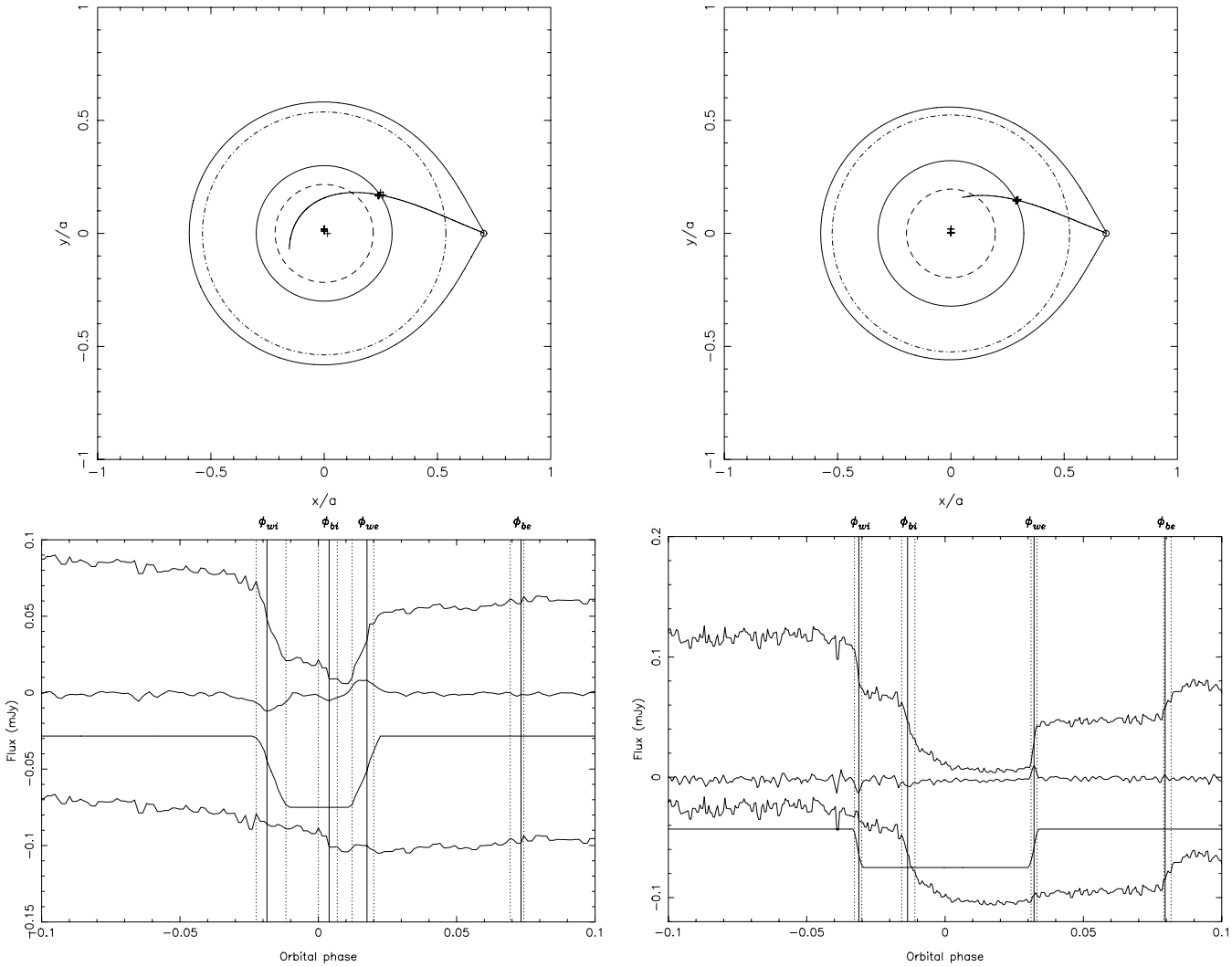

Figure 3. Top row: Trajectory of the gas stream from the secondary star for (left) XZ Eri ($q = 0.117, i = 80.^\circ3$, $R_d/a = 0.300$ and $R_{circ}/a = 0.217$) and (right) for DV UMa ($q = 0.148$, $i = 84.^\circ4$, $R_d/a = 0.322$ and $R_{circ}/a = 0.196$). The Roche lobe of the primary, the position of the inner Lagrangian point L_1 and the disc of radius R_d are all plotted. The positions of the white dwarf and bright-spot light centres corresponding to the observed ingress and egress phases are also plotted. The circularization radius R_{circ} (Verbunt & Rappaport 1988, equation 13) is shown as a dashed circle, and the tidal radius (Paczyński 1977) as a dot-dashed circle. Bottom row: White dwarf deconvolution of (left) the g' band light curve of XZ Eri on 2003 November 13 (cycle 4733) and (right) the g' band light curve of DV UMa on 2003 May 23. Top to bottom: The data after smoothing by a median filter; the derivative after smoothing by a box-car filter and subtraction of a spline fit to this, multiplied by a factor of 1.5 for clarity; the reconstructed white dwarf light curve, shifted downwards by 0.075 mJy; the original light curve minus the white dwarf light curve after smoothing by a median filter, shifted downwards by 0.11 mJy. The vertical lines show the contact phases of the white dwarf and bright-spot eclipses, the dotted lines corresponding to $\phi_{w1}, \ldots, \phi_{w4}, \phi_{b1}, \ldots, \phi_{b4}$ and the solid lines (labelled) to ϕ_{wi}, ϕ_{we} and ϕ_{bi}, ϕ_{be}. The bright-spot ingress and egress are plainly visible in the light curves of both objects, quickly following the white dwarf ingress and egress, respectively.

Table 5. Mean position and extent of the bright-spot as defined in Feline et al. (2004).

	XZ Eri	DV UMa
$\Delta R_d/a$	0.0378	0.0258
$\Delta\theta$	$8.^\circ73$	$7.^\circ57$
$\Delta Z/a$	0.0174	0.0399
$\Delta Z_2/a$	0.0161	0.0217
R_d/a	0.300	0.322
θ	$34.^\circ53$	$27.^\circ47$

(ix) The disc exponent, b, describing the power law of the radial intensity distribution of the disc.

(x) A phase offset, ϕ_0.

The AMOEBA algorithm (downhill simplex; Press et al. 1986) was used to adjust selected parameters to find the best fit. A linear regression was then used to scale the four light curves (for the white dwarf, bright-spot, accretion disc and secondary) to fit the observed light curves in each passband. The data were not good enough to determine the limb-darkening coefficient U_w accurately, so this was held at a typical value of 0.5 for each fit. The disc parameter for DV UMa was held fixed at $b = 1.0$ as it was too faint to be well constrained.

Table 6. Parameters fitted using a modified version of the model of Horne et al. (1994). The fluxes of each component are also shown. XZ Eri has been fitted by phase-folding the two eclipses and binning by two data points. DV UMa has been fitted by phase-folding all three eclipses and binning by two data points. Note that the orbital inclination i is not a fitting parameter but is calculated using q and $\Delta\phi$.

Parameter	XZ Eri			DV UMa		
	u'	g'	r'	u'	g'	i'
Inclination i	$80\overset{\circ}{.}4 \pm 0\overset{\circ}{.}8$	$80\overset{\circ}{.}1 \pm 0\overset{\circ}{.}1$	$80\overset{\circ}{.}4 \pm 0\overset{\circ}{.}2$	$83\overset{\circ}{.}8 \pm 0\overset{\circ}{.}2$	$84\overset{\circ}{.}3 \pm 0\overset{\circ}{.}1$	$84\overset{\circ}{.}3 \pm 0\overset{\circ}{.}1$
Mass ratio q	0.11 ± 0.02	0.116 ± 0.003	0.107 ± 0.002	0.159 ± 0.003	0.1488 ± 0.0011	0.153 ± 0.002
Eclipse phase width $\Delta\phi$	0.0342 $\pm$0.0007	0.03362 $\pm$0.00021	0.0333 $\pm$0.0003	0.06346 $\pm$ 0.00017	0.06352 $\pm$0.00007	0.06307 $\pm$0.00015
Outer disc radius $R_{\rm d}/a$	0.307 $\pm$0.011	0.295 $\pm$0.003	0.316 $\pm$0.005	0.317 $\pm$0.004	0.32278 $\pm$0.00016	0.31272 $\pm$0.00017
White dwarf limb darkening $U_{\rm w}$	0.5	0.5	0.5	0.5	0.5	0.5
White dwarf radius $R_{\rm w}/a$	0.019 $\pm$0.002	0.0175 $\pm$0.0006	0.0195 $\pm$0.0010	0.0091 $\pm$0.0016	0.0092 $\pm$0.0004	0.0082 $\pm$0.0014
Bright-spot scale S/a	0.014 $\pm$0.010	0.013 $\pm$0.002	0.0147 $\pm$0.0008	0.0150 $\pm$0.0010	0.0211 $\pm$0.0002	0.049 $\pm$0.003
Bright-spot orientation $\theta_{\rm B}$	$134\overset{\circ}{.}1 \pm 1\overset{\circ}{.}0$	$141\overset{\circ}{.}9 \pm 0\overset{\circ}{.}3$	$141\overset{\circ}{.}4 \pm 0\overset{\circ}{.}3$	$142\overset{\circ}{.}0 \pm 0\overset{\circ}{.}8$	$137\overset{\circ}{.}75 \pm 0\overset{\circ}{.}09$	$169\overset{\circ}{.}4 \pm 0\overset{\circ}{.}6$
Isotropic flux fraction $f_{\rm iso}$	0.14 ± 0.03	0.140 ± 0.008	0.2294 ± 0.0015	0.157 ± 0.009	0.1989 ± 0.0019	0.262 ± 0.004
Disc exponent b	0.74965	0.4 ± 2.1	0.3 ± 0.3	1	1	1
Phase offset ϕ_0	16×10^{-4} $\pm 3 \times 10^{-4}$	16.3×10^{-4} $\pm 0.8 \times 10^{-4}$	17.0×10^{-4} $\pm 1.2 \times 10^{-4}$	2.5×10^{-4} $\pm 0.9 \times 10^{-4}$	5.48×10^{-4} $\pm 0.10 \times 10^{-4}$	1.7×10^{-4} $\pm 0.7 \times 10^{-4}$
χ^2 of fit	656	897	1554	1059	6873	4332
Number of data points ν	611	611	611	636	636	636
Flux (mJy)						
White dwarf	0.0453 $\pm$0.0011	0.0510 $\pm$0.0004	0.0443 $\pm$0.0004	0.0496 $\pm$0.0008	0.0415 $\pm$0.0002	0.0269 $\pm$0.0004
Accretion disc	0.001 $\pm$0.003	0.0033 $\pm$0.0009	0.0000 $\pm$0.0010	0.0131 $\pm$0.0015	0.0069 $\pm$0.0004	0.0065 $\pm$0.0007
Secondary	0.0020 $\pm$0.0019	0.0029 $\pm$0.0006	0.0064 $\pm$0.0007	0.0027 $\pm$0.0007	0.00531 $\pm$0.00018	0.0680 $\pm$0.0003
Bright-spot	0.0273 $\pm$0.0005	0.03545 $\pm$0.00018	0.0343 $\pm$0.0002	0.0882 $\pm$0.0005	0.0879 $\pm$0.00014	0.1157 $\pm$0.0004

In order to estimate the errors on each parameter once the best fit had been found, we perturbed one parameter from its best-fitting value by an arbitrary amount (initially 5 per cent) and reoptimized the rest of them (holding the parameter of interest, and any others originally kept constant, fixed). We then used a bisection method to determine the perturbation necessary to increase χ^2 by 1, i.e. $\chi^2 - \chi^2_{\rm min} = \Delta\chi^2 = 1$. The difference between the perturbed and best-fitting values of the parameter gave the relevant 1σ error (Lampton, Margon & Bowyer 1976). This procedure failed to find the likely error for the disc exponent b of the u' band of XZ Eri, as the disc flux is small in this case and the light curve noisy, so perturbation of the parameter made virtually no difference to the χ^2 of the fit.

The results of the model fitting are given in Table 6 and shown in Fig. 4. Each colour band was fitted independently, as there were found to be significant differences between many of the optimum parameters for each band. This is to be expected for parameters such as the bright-spot scale S, where one would anticipate that the cooler regions are more extended than the hotter ones (as seen for DV UMa). We would of course expect the mass ratio to remain constant in all three colour bands for each object, which it indeed does.

The results of a white dwarf model atmosphere fit (Bergeron et al. 1995) to the fluxes in each passband are given in Table 7. We have used the white dwarf cooling curves of Wood (1995) for $M_{\rm w}/{\rm M}_{\odot} = 0.75$ (interpolating between 0.7 and 0.8) and $M_{\rm w}/{\rm M}_{\odot} = 1.0$, the approximate masses found using the Nauenberg relation for XZ Eri and DV UMa, to give radial corrections of 7.6 and 7.0 per cent, respectively. These were used to determine the absolute system parameters given in Table 7.

We note that the higher signal-to-noise ratio light curves of the i', r' and g' bands have $\chi^2/\nu \gg 1$ (see Table 6). This is because these data are dominated by flickering, not photon noise, unlike the u' data. If we had enough cycles to remove the effects of flickering completely, we would expect, for an accurate model, to achieve $\chi^2/\nu = 1$.

Since not all of the orbital cycle of DV UMa was observed, the parameters that are constrained by the orbital hump are rather more uncertain for DV UMa than they are for XZ Eri. This may introduce some systematic errors into the estimation of the bright-spot

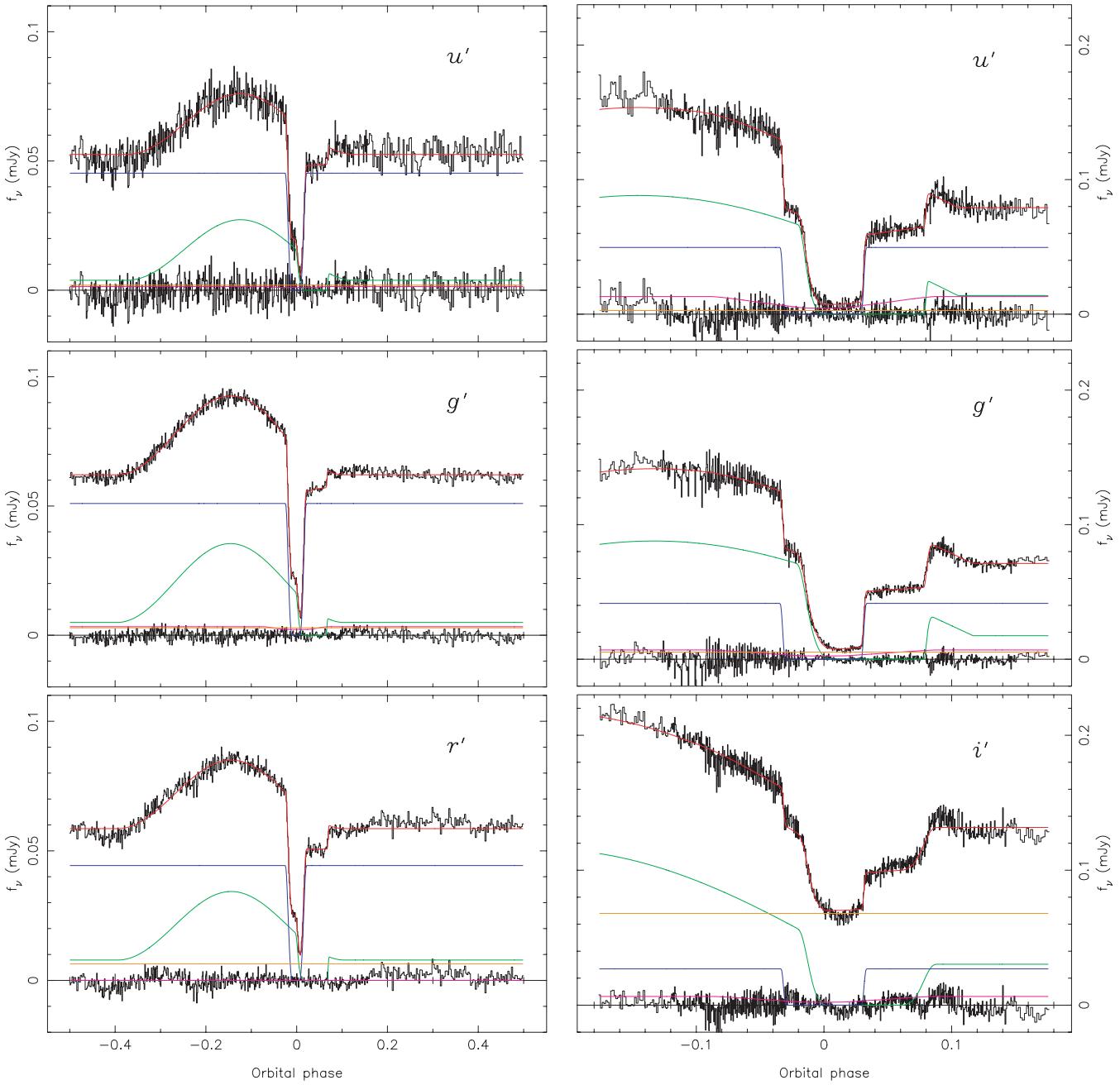

Figure 4. Left: the phase-folded u', g' and r' light curves of XZ Eri, fitted separately using the model described in Section 5.2. Right: the phase-folded u', g' and i' light curves of DV UMa. The data (black) are shown with the fit (red) overlaid and the residuals plotted below (black). Below are the separate light curves of the white dwarf (blue), bright-spot (green), accretion disc (purple) and the secondary star (orange). Note that the disc in both objects is very faint, as is the secondary (except for the i' band of DV UMa).

orientation θ_B and the bright-spot flux. We suspect that the slightly unsatisfactory fit to the i' data of DV UMa during bright-spot egress is due to additional structure superimposed on the orbital hump, causing the bright-spot orientation to be overestimated.

5.3 Comparison of methods

We have determined the system parameters of the eclipsing dwarf novae XZ Eri and DV UMa through two methods: the derivative method of Wood et al. (1986) and the parametrized model technique of Horne et al. (1994). We proceed to compare these two techniques, first noting that the system parameters determined by each (given in Table 7) are reassuringly in good agreement for the most part.

Given data with an excellent signal-to-noise ratio (S/N) and covering many phase-folded cycles, the measurement of the contact phases from the light-curve derivative is capable of producing accurate and reliable results (e.g. Wood et al. 1989). It is less dependable with only a few cycles, however, even if they are individually of high S/N. This is due to flickering having the effect of partially masking the exact location of the contact phases $\phi_1, \ldots, \phi_4$. This problem will affect the values for the deconvolved fluxes of each component and the constraints on the size of the white dwarf

Table 7. System parameters of XZ Eri and DV UMa derived using the Nauenberg mass–radius relation corrected to the appropriate T_w. Here R_r is the volume radius of the secondary's Roche lobe (Eggleton 1983), and R_{min} is as defined by Verbunt & Rappaport (1988, equation 13). The weighted means of the appropriate values from Table 6 are used for the model parameters. Each object has one column of parameters calculated using the derivative method, and one column derived using the parametrized model technique.

	XZ Eri		DV UMa	
Parameter	Derivative	Model	Derivative	Model
Inclination i	$80\overset{\circ}{.}3 \pm 0\overset{\circ}{.}6$	$80\overset{\circ}{.}16 \pm 0\overset{\circ}{.}09$	$84\overset{\circ}{.}4 \pm 0\overset{\circ}{.}8$	$84\overset{\circ}{.}24 \pm 0\overset{\circ}{.}07$
Mass ratio $q = M_r/M_w$	0.117 ± 0.015	0.1098 ± 0.0017	0.148 ± 0.013	0.1506 ± 0.0009
White dwarf mass $M_w/M_\odot$	1.01 ± 0.09	0.767 ± 0.018	1.14 ± 0.12	1.041 ± 0.024
Secondary mass $M_r/M_\odot$	0.119 ± 0.019	0.0842 ± 0.0024	0.169 ± 0.023	0.157 ± 0.004
White dwarf radius $R_w/R_\odot$	0.0082 ± 0.0014	0.0112 ± 0.0003	0.0067 ± 0.0018	0.0079 ± 0.0004
Secondary radius $R_r/R_\odot$	0.147 ± 0.015	0.1315 ± 0.0019	0.207 ± 0.016	0.2022 ± 0.0018
Separation $a/R_\odot$	0.680 ± 0.021	0.619 ± 0.005	0.90 ± 0.03	0.869 ± 0.007
White dwarf radial velocity $K_w/\mathrm{km\,s^{-1}}$	58 ± 8	49.9 ± 0.9	68 ± 6	66.7 ± 0.7
Secondary radial velocity $K_r/\mathrm{km\,s^{-1}}$	496.9 ± 2.0	454.7 ± 0.4	457.5 ± 2.6	443.2 ± 0.5
Outer disc radius R_d/a	0.300 ± 0.017	0.3009 ± 0.0025	0.322 ± 0.011	0.31805 ± 0.00012
Minimum circularization radius R_{min}/a	0.217 ± 0.013	0.2229 ± 0.0014	0.196 ± 0.008	0.1948 ± 0.0005
White dwarf temperature T_w/K	$15\,000 \pm 500$	$17\,000 \pm 500$	$20\,000 \pm 1500$	$20\,000 \pm 1500$

and bright-spot, which are used to determine the individual component masses. The mid-points of ingress and egress, especially those of the white dwarf, are generally still well determined though, since the signal (a peak in the derivative of the light curve) is large due to the rapid ingress and egress of the eclipsed body. This makes the determination of the mass ratio and the orbital inclination relatively simple and reliable. It also means that this technique is well suited to determining the times of mid-eclipse in order to calculate the ephemeris.

We believe that the differences between the component masses and radii of XZ Eri determined by each technique (Table 7) are due to the above effect of flickering. The mass ratios quoted are consistent with each other, but the relative white dwarf radius estimated from the derivative method is somewhat smaller than that determined from the parametrized model ($R_w/a = 0.012 \pm 0.002$ and 0.0181 ± 0.0005, respectively). This also affects the estimates of the component radii and masses.

For the purpose of determining the system parameters, we prefer the parametrized model technique over the derivative method. This is because the former constrains the parameters using all the points in the light curve to minimize χ^2. This procedure has several advantages, as follows.

(i) The value of χ^2 provides a reliable estimate of the goodness of fit, which is used to optimize the parameter estimates. The measurement of the contact phases and subsequent deconvolution of the light curves in the derivative method is not unique (it is affected by the choice of box-car and median filters, for instance), and this technique lacks a comparable merit function.

(ii) Rapid flickering and photon noise during the ingress and/or egress phases are less problematic for the parametrized model as the light curves are evaluated using all the data points, not just the few during ingress and egress.

(iii) The above points indicate that the parametrized model technique requires fewer cycles to obtain accurate results. This is indeed what we found in practice, meaning that this method could be applied to each passband separately to investigate the temperature dependence of each parameter, if any.

(iv) The bright-spot egress in particular is often faint (due to foreshortening) and difficult to reconstruct using the derivative method. The parametrized model method is also likely to be easier to apply to cases where the ingress of the white dwarf and bright-spot are merged, as seen in IP Peg (Wood et al. 1986) and EX Dra (Baptista, Catalán & Costa 2000).

For these reasons, we believe that the results given by the parametrized model of the eclipse are better determined than those of the derivative technique. However, the former method does have some disadvantages. Ideally, it requires observations of most of the orbital cycle, as the orbital hump is needed to fit some parameters reliably. Longer time-scale flickering can also cause some problems if only a few cycles are available. As with any such technique, the key weakness of the parametrized model method is the need for an accurate model. As Fig. 4 shows, apart from the i' band of DV UMa, the residual from the fit shows no large peaks in areas such as the ingress and egress of the white dwarf or bright-spot. Such peaks would be expected if the model were not adequately fitting the data.

6 DISCUSSION

We have presented an analysis of two quiescent eclipses of XZ Eri and three quiescent eclipses of DV UMa. For both objects, separate eclipses of the white dwarf and bright-spot were observed. The identification of the bright-spot ingress and egress is unambiguous in each case. These eclipses have been used to determine the system parameters, given in Table 7, via two independent methods. The first of these is through analysis of the light-curve derivative (Wood et al. 1985, 1986) and the second by fitting a parametrized model of the eclipse (Horne et al. 1994).

The system parameters of DV UMa have also been estimated by Patterson et al. (2000) using eclipse deconvolution. Our analysis is consistent with their findings, but the parametrized model of the eclipse provides much more accurate results. The value we obtain for the mass ratio, for instance, is a factor of $\sim$17 more accurate than that obtained by Patterson et al. (2000). As Patterson et al. (2000) note, the spectral type of the secondary star in DV UMa (M4.5; Mukai et al. 1990) implies $M_r/M_\odot = 0.12$–0.18 for a main-sequence star of solar metallicity (Chabrier & Baraffe 1997; Henry et al. 1999), consistent with our results (Table 7). Mukai et al. (1990) derive the primary temperature and radius of DV UMa from

spectroscopic observations by assuming that the white dwarf emits a blackbody spectrum. The temperature they derive, $T_{\rm w} = 22\,000 \pm 1500$ K, is consistent with our results (Table 7). The primary radius ($R_{\rm w} = 26\,000$ –7700 km) Mukai et al. (1990) calculate is only marginally consistent with our results for the derivative technique and not consistent with the results of the parametrized model. This is probably due to the limitation of assuming a blackbody spectrum (Mukai et al. 1990).

The two quiescent eclipses of XZ Eri have been used to make the first determination of the system parameters for this object, given in Table 7. The mass ratio we derive, $q = 0.1098 \pm 0.0017$, is consistent with XZ Eri being an SU UMa star (Whitehurst 1988; Whitehurst & King 1991), as indicated by its (super)outburst history (Woudt & Warner 2001; Uemura et al. 2004). We also note that the orbital period and mass ratio of XZ Eri are similar to those of OY Car (Wood et al. 1989).

The bright-spot scale S of XZ Eri is constant over all three colour bands. In DV UMa, however, it increases in size as the colour becomes redder. This is easily interpretable: the material cools as it moves farther from the impact region between the accretion disc and the gas stream.

The results from the parametrized model of XZ Eri give a very low secondary star mass of $M_{\rm r}/{\rm M}_{\odot} = 0.0842 \pm 0.0024$. This is close to the upper limit on the mass of a brown dwarf, which is 0.072 $\rm M_{\odot}$ for objects with solar composition, but can be up to 0.086 $\rm M_{\odot}$ for objects with zero metallicity (Basri 2000).

The empirical mass–radius and mass–period relations for the secondary stars of CVs of Smith & Dhillon (1998) are in good agreement with the values determined here. The mass of the white dwarf in XZ Eri is consistent with the mean mass of white dwarfs in dwarf novae below the period gap derived by Smith & Dhillon (1998). The white dwarf in DV UMa, however, is unusually massive. Our assumption that we are observing a bare white dwarf and not a boundary layer around the primary cannot explain this, as the white dwarf mass derived would in this case be a lower limit (e.g. Feline et al. 2004).

Bisikalo et al. (1998) found from numerical simulations that 'bright-spot' eclipse features in CVs may be due to an extended shock wave located on the edge of the stream. Our results do not show any evidence for this. If the bright-spot emission were coming from a region of shocked gas in the stream, then we might expect the bright-spot orientation $\theta_{\rm B}$ to coincide with the flow direction of the stream, which is approximately 169° for XZ Eri and 167° for DV UMa. In fact, apart from the less reliable i' band measurement of DV UMa, the results in Table 6 show that the orientation is half-way between the direction of the stream and disc (approximately 125° for XZ Eri and 118° for DV UMa) flows. The eclipse timings of the bright-spot also show the bright-spot to be extended along the line between the stream and disc trajectories (Fig. 5).

Finally, we note that the system parameters we derive for DV UMa are consistent with the superhump period–mass ratio relation of Patterson (1998). XZ Eri, however, lies 5σ off this relation. We use here the superhump periods $P_{\rm sh} = 0.062\,808 \pm 0.000\,017$ d for XZ Eri (Uemura et al. 2004) and $P_{\rm sh} = 0.088\,70 \pm 0.000\,08$ d for DV UMa (Patterson et al. 2000).

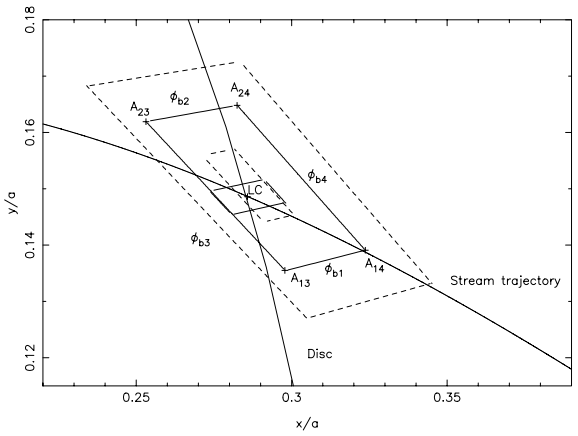

Figure 5. Horizontal structure of the bright-spot of DV UMa for $q = 0.148$, showing the region on the orbital plane within which the bright-spot lies. The light centre LC is marked by a cross, surrounded by the inner solid box, which corresponds to the rms variations in position. The phase arcs which correspond to the bright-spot contact phases are shown as the outer solid box, with the rms variations in position shown as the two dashed boxes. Intersections of the phase arcs $\phi_{{\rm b}j}$ and $\phi_{{\rm b}k}$ are marked A_{jk}, with crosses. The stream trajectory and disc of radius $R_{\rm d} = 0.322a$ are also plotted as solid curves.

ACKNOWLEDGMENTS

We would like to thank Alan Fitzsimmons for giving us some of his valuable telescope time. WJF and CSB are supported by PPARC studentships. TRM acknowledges the support of a PPARC Senior Research Fellowship. ULTRACAM is supported by PPARC grant PPA/G/S/2002/00092. This research has made use of NASA's Astrophysics Data System Bibliographic Services. The work reported here is based on observations made with the William Herschel Telescope operated on the island of La Palma by the Isaac Newton Group in the Spanish Observatorio del Roque de los Muchachos of the Instituto de Astrofisica de Canarias.

REFERENCES

Bailey J. A., 1979, MNRAS, 187, 645
Baptista R., Catalán M. S., Costa L., 2000, MNRAS, 316, 529
Basri G., 2000, ARA&A, 38, 485
Bergeron P., Wesemael F., Beauchamp A., 1995, PASP, 107, 1047
Bisikalo D. V., Boyarchuk A. A., Chechetkin V. M., Kuznetsov O. A., Molteni D., 1998, MNRAS, 300, 39
Chabrier G., Baraffe Y., 1997, A&A, 327, 1039
Cook M. C., Warner B., 1984, MNRAS, 207, 705
Dhillon V. S., Marsh T. R., 2001, New Astron. Rev., 45, 91
Eggleton P. P., 1983, ApJ, 268, 368
Feline W. J., Dhillon V. S., Marsh T. R., Stevenson M. J., Watson C. A., Brinkworth C. S., 2004, MNRAS, 347, 1173
Hamada T., Salpeter E. E., 1961, ApJ, 134, 683
Henry T. J., Franz O. G., Wasserman L. H., Benedict G. F., Shelus P. J., Ianna P. A., Kirkpatrick J. D., McCarthy D. W., 1999, ApJ, 512, 864
Horne K., Marsh T. R., Cheng F. H., Hubeny I., Lanz T., 1994, ApJ, 426, 294
Howell S. B., Mason K. O., Reichart G. A., Warnock A., Kreidl T. J., 1988, MNRAS, 233, 79
Howell S. B., Szkody P., Kreidl T. J., Dobrzycka D., 1991, PASP, 103, 300
Koester D., Schönberner D., 1986, A&A, 154, 125
Lampton M., Margon B., Bowyer S., 1976, ApJ, 208, 177
Mukai K. et al., 1990, MNRAS, 245, 385
Nauenberg M., 1972, ApJ, 175, 417
Nogami D., Kato T., Baba H., Novák R., Lockley J., Somers M., 2001, MNRAS, 322, 79
Paczyński B., 1977, ApJ, 216, 822
Patterson J., 1998, PASP, 110, 1132

Patterson J. et al., 2000, PASJ, 112, 1584
Press W. H., Flannery B. P., Teukolsky S. A., Vetterling W. T., 1986, Numerical Recipes in Fortran. Cambridge Univ. Press, Cambridge
Shapley H., Hughes E. M., 1934, Ann. Harvard Coll. Obs., 90, 163
Smith D. A., Dhillon V. S., 1998, MNRAS, 301, 767
Smith J. A., Tucker D. L. et al., 2002, AJ, 123, 2121
Szkody P., Howell S. B., 1992, ApJS, 78, 537
Uemura M. et al., 2004, PASJ, 56, S141
Verbunt F., Rappaport S., 1988, ApJ, 332, 193
Warner B., 1995, Cataclysmic Variable Stars. Cambridge Univ. Press, Cambridge
Whitehurst R., 1988, MNRAS, 232, 35
Whitehurst R., King A., 1991, MNRAS, 249, 25
Wood J. H., Irwin M. J., Pringle J. E., 1985, MNRAS, 214, 475
Wood J. H., Horne K., Berriman G., Wade R., O'Donoghue D., Warner B., 1986, MNRAS, 219, 629
Wood J. H., Horne K., Berriman G., Wade R., 1989, ApJ, 314, 974
Wood M. A., 1995, in Koester D., Werner K., eds, Lecture Notes Phys., Vol. 443, European Workshop on White Dwarfs. Springer, Berlin, p. 41
Woudt P. A., Warner B., 2001, MNRAS, 328, 159

This paper has been typeset from a TEX/LATEX file prepared by the author.